

# A Torque Vectoring Optimal Control Strategy for Combined Vehicle Dynamics Performance Enhancement and Electric Motor Ageing Minimisation<sup>\*</sup>

Angelos Kampanakis, Efstathios Siampis,  
Efstathios Velenis and Stefano Longo

*Cranfield University, Cranfield, Bedfordshire, MK43 0AL UK  
(e-mail: kampanakis.a@gmail.com, e.siampis@cranfield.ac.uk,  
e.velenis@cranfield.ac.uk, s.longo@cranfield.ac.uk)*

---

**Abstract:** In this paper we propose a control architecture that combines velocity, sideslip angle and yaw rate regulation with motor temperature regulation on a electric vehicle with four independent electric motors. The linear controller incorporates both the vehicle dynamics and the electric motor dynamics by combining a four-wheel vehicle model with a motor degradation model. It is found that the resulting controller not only enhances the vehicle stability of the vehicle, but also extends the lifetime of motors by regulating their temperatures.

*Keywords:* automotive control; electric vehicles; quadratic regulators; motor control

---

## 1. INTRODUCTION

The rising ecological sensitivity along with the ever tighter government regulations has driven the automotive industry and academia to look for more fuel efficient transport solutions that produce less emissions. One of the current aims of this research is the development of Electric Vehicles (EV) as a viable, cost effective solution. The use of electric motors has distinctive advantages over a conventional driveline such as fast response and high energy efficiency, and in an electric vehicle topology such as the one considered here with four independent electric motors it can dramatically change the behaviour of the vehicle in a positive way by controlling both the direction and magnitude of the torques on the wheels, a method commonly known as torque vectoring. However, using electric motors in an automotive environment also poses specific problems which are mainly connected to safety and cost issues. In particular, motor degradation is of great importance since it can lead to complete motor failure: while this can occur due to mechanical, thermal, chemical and electrical reasons as pointed by Thorsen and Dalva (1995), studies reveal that more than 90% of electric drives fail due to overheating in the windings insulation or excessive mechanical stresses on the bearings, see Rahman et al. (2010) and Haifang et al. (2011). Especially the insulation temperature of a motor is considered of vital importance since, even for motors with a insulation class  $H$ , a temperature rise of  $10^{\circ}\text{C}$  above  $160^{\circ}\text{C}$  can lead to halving the residual lifetime of the motor. Predicting these issues at the development stage is considered crucial for developing highly optimized electric machines, but a very effective way to reduce the likelihood

of failure is to prevent overheating of the motor during operation. Based on this observation the main goal of this paper is to develop a control strategy that regulates both the vehicle dynamics according to the driver's commands and the motor temperatures to prevent overheating by using the torque vectoring capabilities of a Four Wheel Drive (FWD) electric vehicle.

The study of electric motor degradation for use on electric vehicles has so far progressed independently from the development of active vehicle dynamics systems. Motor degradation surveys deal mainly with the residual lifetime of an electric motor based on temperature and focus on conducting thermal analysis on the motor before it is assembled from its different components, as found in Kimotho and Hwang (2011), Driesen et al. (2001) and Fodorean and Miraoui (2008). Use of Computational Fluid Dynamics (CFD) suites in such studies provides good estimations not only for the steady state temperature, but also for short term overloads. On the other hand extensive research has been carried out on vehicle stability control on Hybrid Electric Vehicles (HEV) and EVs with a variety of control methodologies, ranging from Model Predictive Control (MPC) strategies and Linear Quadratic Regulators (LQR) as found in Siampis et al. (2013), to simpler ones such as Proportional-Integral-derivative (PID) controllers, see Pinto et al. (2010). All of these studies aim to achieve not only better drivability, but also safer operation of the vehicle near the limits of lateral acceleration, but neglect to take into account the effect of high operational motor temperatures on the life of the motor.

In this paper we propose an optimal control strategy that combines a vehicle dynamics model with an electric drive thermal-degradation model to both achieve better vehicle performance and extend the motor life by optimally dis-

---

<sup>\*</sup> The authors would like to acknowledge the financial support from EPSRC via the 'FUTURE Vehicle' project (grant number EP/I038586/1) and the Impact Acceleration Account (grant number EP/K503927/1).

tributing the torques on the four wheels of a FWD electric vehicle. After introducing the vehicle, tyre and motor models to be used, the optimal control strategy is explained. Finally, simulation results show the effectiveness of the proposed solution under both normal driving conditions and a critical turn.

## 2. VEHICLE AND MOTOR MODELS

In this section we introduce the vehicle and tyre models, along with the motor model which will be used to provide the life expectancy of the four electric motors.

### 2.1 Vehicle and Tyre Model

The vehicle and tyre models used in this paper are similar to the one found in Siampis et al. (2013), where the interested reader can refer for more details. The equations of motion for a vehicle travelling on a horizontal plane are (Fig. 1):

$$\begin{aligned} m\dot{V} &= (f_{FLx} + f_{FRx}) \cos(\delta - \beta) \\ &\quad - (f_{FLy} + f_{FRy}) \sin(\delta - \beta) \\ &\quad + (f_{RLx} + f_{RRx}) \cos \beta \\ &\quad + (f_{RLy} + f_{RRy}) \sin \beta, \end{aligned} \quad (1)$$

$$\begin{aligned} \dot{\beta} &= \frac{1}{mV} [(f_{FLx} + f_{FRx}) \sin(\delta - \beta) \\ &\quad + (f_{FLy} + f_{FRy}) \cos(\delta - \beta) \\ &\quad - (f_{RLx} + f_{RRx}) \sin \beta \\ &\quad + (f_{RLy} + f_{RRy}) \cos \beta] - \dot{\psi}, \end{aligned} \quad (2)$$

$$\begin{aligned} I_z \ddot{\psi} &= \ell_F [(f_{FLy} + f_{FRy}) \cos \delta \\ &\quad + (f_{FLx} + f_{FRx}) \sin \delta] - \ell_R (f_{RLy} + f_{RRy}) \\ &\quad + w_L (f_{FLy} \sin \delta - f_{FLx} \cos \delta - f_{RLx}) \\ &\quad + w_R (f_{FRx} \cos \delta - f_{FRy} \sin \delta + f_{RRx}) \end{aligned} \quad (3)$$

$$I_w \dot{\omega}_{ij} = T_{ij} - f_{ijx} r, \quad i = F, R, j = L, R. \quad (4)$$

where  $m$  and  $I_z$  are the mass of the car and the moment of inertia about the vertical axis respectively,  $V$  is the velocity at the center of mass,  $\beta$  and  $\psi$  are the sideslip and yaw angle of the vehicle.  $I_w$  is the moment of inertia of each wheel about its axis,  $r$  is the wheel radius and  $\omega_{ij}$  is the angular speed of each wheel ( $i$  is marking the Front or Rear wheels and  $j$  the Left and Right). The steering angle is  $\delta$  and  $T_{ij}$  is the applied torque to each wheel;  $f_{ijk}$  are the longitudinal and lateral forces which are stressed on the wheel during the driving conditions and  $\ell_F, \ell_R, w_L, w_R$  are the distances of each wheel from the center of mass.

The tyre forces  $f_{ijk}$  in the above equations are described in this paper using the Magic Formula from Pacejka and Bakker (1991). Assuming, for simplification reasons, that the camber and toe angles at each wheel are zero, the tyre forces can be found as functions of the longitudinal and lateral slips

$$s_{ijx} = \frac{V_{ijx} - \omega_{ij} r_{ij}}{\omega_{ij} r_{ij}}, \quad s_{ijy} = \frac{V_{ijy}}{\omega_{ij} r_{ij}}, \quad (5)$$

where  $V_{ijk}$  ( $i = F, R, j = L, R, k = x, y$ ) is the

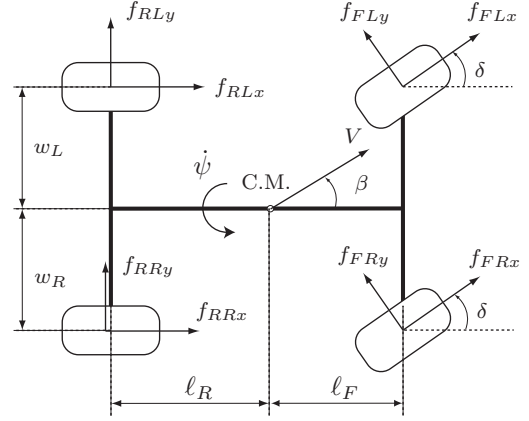


Fig. 1. Four-wheel vehicle model.

longitudinal velocity at the center of each of the four wheels. If we also assume a linear dependence of the tyre friction forces to the normal forces acting on each tyre, we get

$$\mu_{ij} = f_{ij}/f_{ijz}, \quad \mu_{ijk} = f_{ijk}/f_{ijz}, \quad (6)$$

where  $f_{ij} = \sqrt{f_{ijx}^2 + f_{ijy}^2}$  is the total friction force acting on each tyre,  $\mu_{ij}$  is the total tyre force coefficient,  $\mu_{ijk}$  are the longitudinal and lateral tyre force coefficients, and  $f_{ijz}$  are the vertical forces on each of the four wheels. The total tyre force coefficient is calculated using the MF

$$\mu_{ij}(s_{ij}) = MF(s_{ij}) = D \sin(C(\text{atan}(Bs_{ij}))), \quad (7)$$

where  $s_{ij} = \sqrt{s_{ijx}^2 + s_{ijy}^2}$ . Then, assuming symmetric tyre characteristics in the longitudinal and lateral direction, we can find the longitudinal and lateral tyre force coefficients using the friction circle equations

$$\mu_{ijk} = -\frac{s_{ijk}}{s_{ij}} \mu_{ij}(s_{ij}). \quad (8)$$

Finally, neglecting the pitch and roll rotation along with the vertical motion of the sprung mass of the vehicle, the vertical forces  $f_{ijz}$  on each wheel can be found using the static load distribution on the car and the longitudinal/lateral load transfer caused from longitudinal and lateral acceleration. Taking for example the front-left wheel the vertical tyre force is

$$f_{FLz} = f_{FLz}^0 - \Delta f_L^x - \Delta f_F^y, \quad (9)$$

where the static load is given by

$$f_{FLz}^0 = \frac{m g \ell_R, w_R}{(\ell_F + \ell_R)(w_L + w_R)}, \quad (10)$$

and the longitudinal load transfer is given as a function of the longitudinal acceleration by

$$\Delta f_L^x = \frac{m h w_R}{(\ell_F + \ell_R)(w_L + w_R)} a_x, \quad (11)$$

where  $h$  the distance from the Center of Mass of the

vehicle from the road surface and  $a_x$  is the longitudinal acceleration of the vehicle.

## 2.2 Motor Model

A plethora of Permanent Magnet (PM) motor models can be found in the literature, see Yang et al. (2014), Cvetkovski et al. (2004) and Jun and Yiming (2011). Most of these models are high-fidelity models incorporating not only torque, speed, voltage and current inputs, but also offering insights on the flux, emf and inverter characteristics of the motor. However, in the context of this paper, such a highly detailed model is unnecessarily complex and a simple model as the one found in Pillay and Krishnan (1989) is employed for modeling the motor behavior: the system inputs are set as the angular velocity  $\omega$  of the rotor and the load torque  $\tau_L$  and the outputs are set as the electric torque  $\tau_e$ , the input power  $P_{inp}$  and the current  $I$ . Consequently, the current and input power of the motor are derived from the basic voltage and current equations for the PM motor:

$$V_q = RI_q + \frac{d(L_q I_q)}{dt} + \omega_s \lambda_d, \quad (12)$$

$$V_d = RI_d + \frac{d(L_d I_d)}{dt} - \omega_s \lambda_q, \quad (13)$$

$$P_{inp} = \frac{3}{2}(V_d I_d + V_q I_q), \quad (14)$$

where  $V_q$  and  $V_d$  are the voltages,  $I_d$  and  $I_q$  are the currents,  $\lambda_q$  and  $\lambda_d$  are the stator flux linkages and  $L_q$  and  $L_d$  are the inductances of the direct and quadrature axis (d-q axis) of the motor respectively. Furthermore,  $R$  is the stator resistance and  $\omega_s$  the inverter frequency which is given by  $\omega_s = P\omega$  with  $P$  the number of pair poles of the motor. The electric torque equation of the motor is a function of the two axis currents and is given by

$$\tau_e = \frac{3}{2}P[\lambda_{af} I_q + (L_d - L_q) I_d I_q], \quad (15)$$

where  $\lambda_{af}$  is the flux linkage of the stator to the rotor magnets. If we assume that the current in the d-axis is the reference (Fig. 2) and is forced to be zero, the current for the q-axis is given from:

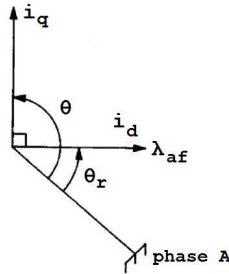


Fig. 2. Current phase diagram.

$$\tau_e = K_t I_q, \quad (16)$$

$$K_t = \frac{3}{2}P\lambda_{af} I_q, \quad (17)$$

The linkage between the load and electric torque is made from the following relationship:

$$\tau_e = \tau_L + B\omega + \frac{d(\omega)}{dt} J, \quad (18)$$

where  $J$  and  $B$  are the motor moment of inertia and damping coefficient respectively. Finally assuming the back emf of the motor to be negligible,  $V_d = 0$  and the power required to the motor reduces to  $P_{inp} = V_q I_q$ .

As already mentioned in the *Introduction* section, the lifetime of the motors will be measured through its temperature. According to Pyrhonen et al. (2008), losses in PM motors occur due to copper  $P_{cu}$ , mechanical  $P_{mech}$  and iron  $P_{fe}$  losses, with the first two calculated from the following equations

$$P_{cu} = I^2 R, \quad (19)$$

$$P_{mech} = B\omega, \quad (20)$$

while the iron losses can be derived from the power balance formula from Katsumi and Yoshiaki (2006)

$$\begin{aligned} P_{fe} &= P_{inp} - P_{mech} - P_{cu} - P_{out} \\ &= VI - b\omega - I^2 R - \tau\omega. \end{aligned} \quad (21)$$

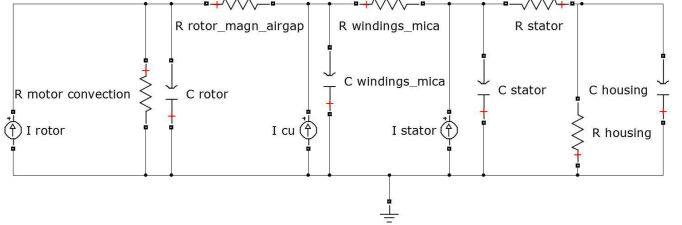


Fig. 3. Temperature lumped parameters model.

For the temperature estimation in this paper we propose a thermal-electric equivalent lumped parameters model (Fig. 3). Thermal resistances are the elements opposing the heat transfer, capacitors correspond to heat capacities (the heat accumulated by each material) and sources to heat origin-losses. The model is based on the conduction and convection of the materials and radiation heat mechanism is assumed negligible. Following Ohm's Law, the equations for the thermal-electric equivalent model are

$$\Delta T [K] \leftrightarrow \Delta V [V]$$

$$Q [W] \leftrightarrow i [A], \quad (22)$$

$$R = \frac{\Delta V}{I}, \quad (23)$$

$$C = \rho c_p V_m, \quad (24)$$

$$P = \frac{\Delta T}{R}, \quad (25)$$

where  $\Delta T$  is the temperature difference,  $Q$  is heat,  $\rho$  is the material density,  $c_p$  the specific heat of the material and  $V_m$  the volume of the component. A linear state space model of the thermal-electric dynamics (22)-(25) is

$$\begin{bmatrix} \dot{T}_{rot} \\ \dot{T}_{ins} \\ \dot{T}_{sta} \\ \dot{T}_{hous} \end{bmatrix} = CR_A \begin{bmatrix} T_{rot} \\ T_{ins} \\ T_{sta} \\ T_{hous} \end{bmatrix} + CR_B \begin{bmatrix} I_r \\ I_{cu} \\ I_{st} \end{bmatrix}, \quad (26)$$

where  $T_{rot}$ ,  $T_{ins}$ ,  $T_{sta}$  and  $T_{hous}$  are the temperatures of the rotor, insulation, stator and housing of the motor respectively,  $I_{cu}$  are the copper losses of windings, and  $I_{st}$  and  $I_r$  are the combined losses of the stator and rotor.  $CR_A$  is a real  $4 \times 4$  matrix derived from the resistors and capacitors of the electric circuit, while  $CR_B$  is  $4 \times 3$  matrix.

### 3. CONTROL DESIGN

Following Siampis et al. (2013), the proposed control architecture will stabilise the vehicle during emergency situation using combined velocity, slip and yaw rate regulation. However, the controller will also maintain the temperature level on each of the four motors as low as possible by optimally distributing the torques on the four wheels.

From the vehicle model (1) and motor temperature model (26) linearized about the current state, we have

$$\frac{dx}{dt} = \mathbf{A}x + \mathbf{B}u, \quad \mathbf{y} = \mathbf{C}x, \quad (27)$$

where  $\mathbf{A}$  and  $\mathbf{B}$  are the Jacobian matrices from linearization of (1)-(4) and (26),  $\mathbf{C} = \mathcal{I}^{23 \times 23}$  and

$$\mathbf{x} = \begin{bmatrix} V - V^{tar} \\ \beta - \beta^{tar} \\ \dot{\psi} - \dot{\psi}^{tar} \\ \omega_{ij} - \omega_{ij}^{tar} \\ T_{ij_{rot}} - T_{ij_{rot}}^{tar} \\ T_{ij_{ins}} - T_{ij_{ins}}^{tar} \\ T_{ij_{sta}} - T_{ij_{sta}}^{tar} \\ T_{ij_{hous}} - T_{ij_{hous}}^{tar} \end{bmatrix} (23 \times 1), \quad \mathbf{u} = [\tau_{ij} - \tau_{ij}^{tar}]_{(4 \times 1)},$$

with  $\tau_{ij}$  the four torques at the wheels. The optimal control law is then given by

$$\mathbf{u} = \mathbf{R}^{-1} \mathbf{B}^T \mathbf{P}, \quad (28)$$

where  $\mathbf{P}$  is the solution of the associated algebraic Riccati equation and minimizes the quadratic cost

$$\mathcal{J} = \int_0^\infty [\mathbf{y}(t)^T \mathbf{Q} \mathbf{y}(t) + \mathbf{u}(t)^T \mathbf{R} \mathbf{u}(t)] dt,$$

with  $\mathbf{Q}$  and  $\mathbf{R}$  the real symmetric weighting matrices on the output error and the control effort respectively.

### 4. SIMULATIONS

In this section the optimal torque vectoring control system presented above is tested on the nonlinear vehicle-tyre model (1)-(11) along with the motor-temperature model (12)-(25) in Simulink environment under two different simulation scenarios: the first scenario examines the controller's capabilities in regulating the motors' temperatures under normal driving conditions, while the second scenario checks the controller's trade-off between the vehicle dynamics control and motor temperature control in an extreme manoeuvre. In both scenarios the maximum torque limit according to the static torque map of the

Table 1. Vehicle and tyre parameters.

Parameter	Value	Parameter	Value
$m$ (kg)	1420	$\ell_F$ (m)	1.01
$I_z$ (kgm <sup>2</sup> )	1028	$\ell_R$ (m)	1.452
$I_w$ (kgm <sup>2</sup> )	0.6	$r$ (m)	0.298
$w_L$ (m)	0.81	$B$	24
$w_R$ (m)	0.81	$C$	1.5
$h$ (m)	0.317	$D$	0.9

motor used is taken into account, the tyre/road friction coefficient is assumed to be constant at  $\mu = 0.8$ , and the vehicle and tyre parameters are set as in Table 1.

#### 4.1 Normal Driving Scenario

In the first simulation scenario the driver joins a highway road by a) accelerating while cornering through the motorway's entry for 4s and b) bringing the steering command to zero while continuing accelerating in a straight line for 11s after have joined the highway. The initial speed is set to 50kph, while we also assume that all motors have the same initial temperature.

Fig. 4 shows the velocity and yaw rate time histories for the vehicle equipped with the proposed torque vectoring system and, for comparison, the results for a vehicle without a torque vectoring system. As we can see from the plots, both vehicles achieve the same performance for this scenario. However, from Fig. 5 we can conclude that the vehicle with the torque vectoring system achieves this result while also keeping the motors' temperatures at the same levels.

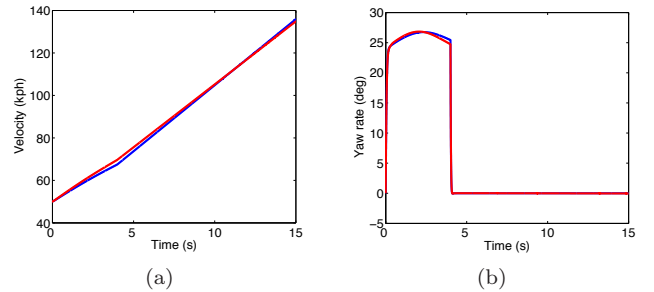


Fig. 4. Velocity and yaw rate time histories for the normal driving scenario. The blue lines correspond to the uncontrolled vehicle and red lines to the vehicle with the proposed torque vectoring system.

#### 4.2 Extreme Turn Scenario

In the second scenario the car is traveling at a high speed and the driver suddenly steers to the left. The initial speed of the vehicle is assumed to be 120km/h while the applied step steering input to the wheels is set to 10deg. The motor temperatures just before the steering command are assumed to have reached steady state conditions while we also assume that no acceleration/brake commands come from the driver.

Fig. 6 shows the velocity and yaw rate time histories for the vehicle equipped with the proposed torque vectoring system and, for comparison, the results for a vehicle that does not regulate the motors' temperatures as in

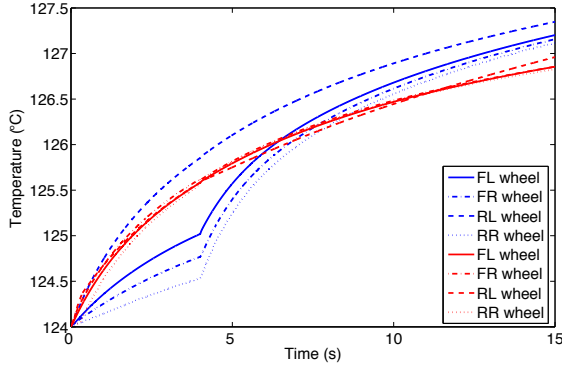


Fig. 5. Motors' temperatures for the normal driving scenario. The blue lines correspond to the uncontrolled vehicle and red lines to the vehicle with the proposed torque vectoring system.

Siampis et al. (2013) and a vehicle without a torque vectoring system. Both the controlled vehicles give a much better vehicle response when compared to the uncontrolled vehicle which exhibits velocity and yaw rate oscillations, but with some distinctive differences (Fig. 7). Since the stability controller neglects the motor temperatures and puts all the effort to bring the car to steady yaw rate, it pushes the motors to their limits (Fig. 7). The temperature and stability controller on the other hand manages to keep the motor temperatures to operational levels with only a small drop in performance when compared to the stability controller.

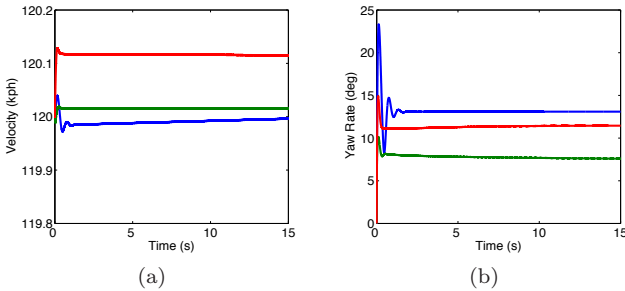


Fig. 6. Velocity and yaw rate time histories for the extreme turn scenario. The blue lines correspond to the uncontrolled vehicle, the red lines to the vehicle with the proposed torque vectoring system, and the green lines to a controller that does not regulate the motors temperatures.

## 5. CONCLUSION

In this paper we presented a torque vectoring control system that combines velocity, yaw rate and sideslip angle regulation with motor temperature regulation to achieve better vehicle stability performance while at the same time extending the life of the motors. Testing the proposed solution in a normal driving scenario confirmed that the controller optimally distributes the torques on the four electric motors to achieve lower overall motor temperatures and equal motor degradation. Furthermore, under a aggressive manoeuvre the controller manages to keep the motor temperatures low with only a small compromise in the driving performance.

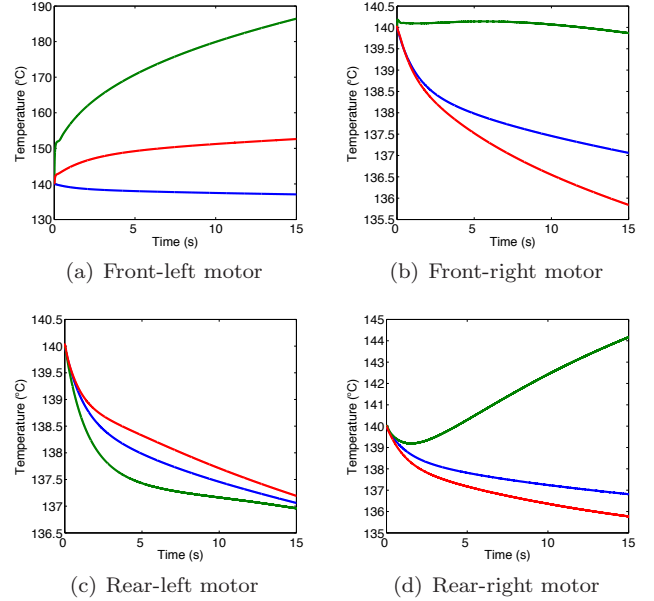


Fig. 7. Temperature time histories for the extreme turn scenario. The blue lines correspond to the uncontrolled vehicle, the red lines to the vehicle with the proposed torque vectoring system, and the green lines to a controller that does not regulate the motors temperatures.

## REFERENCES

- Cvetkovski, G., Petkovska, L., and Cundev, M. (2004). Pm disc motor modelling and simulation for transient analysis. In *IEEE Power Electronics and Motion Control Conference*, volume 2, 577–582. Xi'an, China.
- Driesen, J., Belmans, R., and Hameyer, K. (2001). Finite-element modeling of thermal contact resistances and insulation layers in electrical machines. *IEEE transaction on Industry Applications*, 37(1), 15–20.
- Fodorean, D. and Miraoui, A. (2008). Permanent magnets thermal operation limits in a hybrid excited synchronous machine used on wide speed applications. In *IEEE Optimization of Electrical and Electronic Equipment*, 21–26. Brasov, Romania.
- Haifang, Y., Zhiqiang, L., and Shumei, C. (2011). Research on fault analysis and diagnosis of pmsm in hev. In *Electrical Machines and Systems (ICEMS)*, 1–4. Beijing, China.
- Jun, R. and Yiming, L. (2011). Modeling and simulation of the double-closed loop control system of counter rotating permanent magnet brushless dc motor. In *IEEE Electronic and Mechanical Engineering and Information Technology*, volume 7, 3309–3313. Harbin, Heilongjing, China.
- Katsumi, Y. and Yoshiaki, S. (2006). Iron loss analysis of interior permanent-magnet synchronous motors variation of main loss factors due to driving condition. *IEEE Transactions on Industry Applications*, 42, 1045–1052.
- Kimotho, J. and Hwang, P. (2011). Thermal management of electric vehicle bldc motor. In *SAE Society of Automotive Engineers*. New York, USA.
- Pacejka, H. and Bakker, E. (1991). The magic formula tyre model. In *Proceedings of 1st International Colloquium on Tyre Models for Vehicle Dynamics Analysis*. Delft,

The Netherlands.

- Pillay, P. and Krishnan, R. (1989). Modeling, simulation, and analysis of permanent-magnet motor drives, part i: The permanent-magnet synchronous motor drive. *IEEE Transactions on Industry Applications*, 25, 265–273.
- Pinto, L., Aldworth, S., Watkinson, M., Jeary, P., and Franco-Jorge, M. (2010). Advanced yaw motion control of a hybrid vehicle using twin rear electric motors. In *10th International Symposium on Advanced Vehicle Control*. Loughborough, UK.
- Pyrhonen, J., Jokinen, T., and Hrabovcova, V. (2008). *Design of Rotating Electrical Machines*. John Wiley and Sons, Inc., New York.
- Rahman, M., Azam, T., and Saha, S. (2010). Motor fault detection using vibration patterns. In *International Conference on Electrical and Computer Engineering*, 486–489. Dhaka, Bangladesh.
- Siampis, E., Velenis, E., and Massaro, M. (2013). Electric rear axle torque vectoring for combined yaw stability and velocity control near the limit of handling. In *Decision and Control CDC Conference*, 1552–1557. Firenze, Italy.
- Thorsen, O. and Dalva, M. (1995). A survey of faults on induction motors in offshore oil industry. *IEEE transaction on Industry Applications*, 31(5), 1186–1196.
- Yang, L., Jianwei, Z., Konghui, G., and Jilin, U. (2014). An accurate modeling for permanent magnet synchronous wheel motor including iron loss. *SAE International Journal of Alternative Power*, 105–112.